NUCLEAR INSTRUMENTS AND METHODS 154 (1978) 271-277 ; © NORTH-HOLLAND PUBLISHING CO.

A WIDE BAND ELECTRON SPECTRUM ANALYZER

M. KOMMA

Physikalisches Institut der Universität Tübingen, 7400 Tübingen, Germany

Received 19 September 1977 and in revised form 3 February 1978

An optimization procedure for the design of an electron spectrum analyzer (ELSA), which consists of the combination of a triple focusing magnet with an energy sensitive detector was developed. The resulting magnet focuses a solid angle of 7.6 msr ($5^\circ \times 5^\circ$) and a momentum band of $\Delta p/p = 490\%$ ($p_{max}/p_{min} = 5.9$) into a circle with less than 10 mm ∅, so that small SB-detectors with correspondingly good resolution can be applied. Since ELSA can observe electrons within a wide energy band (e.g. 10–275 keV) and with very low background, it may be a helpful device in scattering experiments such as (e, 2e), (e, eγ) and (e, 2eγ) as well as for conversion electron measurements.

1. Introduction

Two outstanding problems in charged particle spectroscopy are the elimination of intense but undesired parts of a spectrum on the one hand and keeping the spectrum free from the background of other particles on the other. For instance the measurement of conversion electrons requires the selection of γ-quanta and positrons. Or, if one wants to measure inelastically scattered electrons, the overwhelming part of the elastically scattered electrons, in addition to the low energy bremsstrahlung, must be prevented from reaching the detector. The usual way to meet these requirements is to select a single kind of particle as well as a single particle energy by means of a magnetic spectrometer. Furthermore, this method offers good resolution. However, the advantages of good resolution must be paid for with long measuring times, since only one point of the spectrum can be recorded at a time. Although the data collection can be accelerated by sweeping the spectrometer current in on-line measurements[1]), it remains a tempting goal, to avoid the loss of information as far as possible. Thanks to the improved resolution data of Si(Li)- and SB-detectors the simultaneous detection of particles with quite different energies can be realized, if one succeeds in focusing the whole spectrum and a sufficiently large solid angle onto a small area (which means triple focusing). After that the discrimination of unwanted particles can be performed by proper slits and proper shielding of the detector.

In practice the solution of the problem is often complicated by the experimental conditions or the existing apparatus and therefore seems to be impossible at first glance. However, precisely in these cases the present work may be encouraging, since it offers a flexible procedure for the design of a triple focusing magnet which is adapted to a given experimental arrangement. Concerning our experiments[2]), the magnet had to have the following specifications:

- transfer of electrons with energy from 50 to 250 keV
- acceptance of a solid angle of about $5^\circ \times 5^\circ$,
- maximum diameter of focus less than 10 mm, to take advantage of the higher resolution of small detectors,
- image and object distances less than 15 cm (due to the scattering chamber diameter of 50 cm, which makes the employment of an achromatic magnet *system* illusory),
- no distortion of the detection of the remaining particles.

The optimization is divided into three steps: linear optimization (section 2), numerical calculation of the particle trajectories (section 3) and experimental testing of the magnet (section 4). A concluding discussion is given in section 5.

2. Linear optimization of the achromatic dipole magnet (LOAD)

2.1. Triple focusing

The linear theory for deflecting magnets is treated in a variety of textbooks, e.g. refs. 3 and 7), and only those results, that are necessary for the design of a triple focusing magnet will be mentioned here.

If a particle leaves the origin of the object coordinate system (in) with the slopes x'_{in}, y'_{in} and the momentum $p_0 + \delta p_0$, its coordinates in the im-

age coordinate system (out) are to first order:

$$x_{out} = (h_{12}x'_{in} + h_{13}\delta)\cdot R_0,$$
$$y_{out} = v_{12}y'_{in}R_0. \quad (1)$$

Therefore, triple focusing occurs if

$$h_{12} = h_{13} = v_{12} = 0, \quad (2)$$

with

$$h_{12} = a\cos(\varphi-\alpha)/\cos\alpha + \sin\varphi - ab\sin(\varphi-\alpha-\beta)/(\cos\alpha\cos\beta) + b\cos(\varphi-\beta)/\cos\beta,$$
$$h_{13} = 1-\cos\varphi + b[\sin\varphi + (1-\cos\varphi)\tan\beta],$$
$$v_{12} = a(1-\varphi\tan\alpha) + \varphi + ab(\varphi\tan\alpha\tan\beta - \tan\alpha - \tan\beta) + b(1-\varphi\tan\beta).$$

The object and image distances, $a = A/R_0$ and $b = B/R_0$ respectively, are normalized to the radius R_0 of the central ray. The deflection angle is φ, and α and β are the entrance and exit angles. A schematic diagram of the above situation can be found in fig. 1 of ref. 8.

In the general case the matrix elements depend on the six quantities a, α, φ, β, b and n (the field index). I have chosen to assign $n = 0$, which means a homogeneous field. This choice is preferred because an inhomogeneous field enables double focusing only for $0 < n < 1$, in which case energetic focusing with a single-sector magnet is no longer simple*. Thus, after imposing the three conditions (2), there remain two free parameters for the *design* of a triple focusing magnet by means of the *solution* of system (2). This possibility was used by H. Ejiri et al.[5]) at the same time this work was done. They employed the first-order condition for zero-dispersion quoted by R. A. Alvarez et al.[6]) and chose $\varphi = 270°$. This value represents a practical deflection angle which facilitates the isolation of the detector from the source. The same argument concerning the choice of φ is already given by H. A. Enge[7]) for the case of a parallel beam entering a magnet with $h_{11} = h_{13} = v_{11} = 0$. For the present experiment, however, a more generalized treatment of the problem became necessary because of the desired wide momentum band.

The transcendental equations (2) are quite unwieldy, and therefore it is customary to solve them by means of a computer using iterative methods. The result of the calculations is then reported in a diagram which relates the parameter values [R. Ciuti et al.[8])]. Nevertheless, from a purely mathematical point of view, one might expect that the *optimization* with the *boundary condition (2)* is in principle possible. Unfortunately the linear theory is limited to small deviations from the central ray, so that this optimization would fail for large values of $|\delta|$.

Instead, I have introduced a condition for zero-dispersion which holds for any δ and have estimated the focusing properties by means of h_{12} and v_{12}. With this basic assumption the matrix elements for horizontal and vertical focusing are only minimized and not set to zero a priori. Since this new concept requires an optimization procedure, it implies that none of the five parameters may be arbitrarily fixed.

2.2. Exact energetic focusing

If it is assumed that the magnetic field drops to zero at the mechanical boundary of the pole piece – that is, the Sharp-Cutoff-Fringing-Field (SCOFF) approximation – the problem of energetic focusing can be solved in a purely geometrical way. If the shape of the exit boundary is described by the curve (3), one obtains *exact* (therefore the index ex) energetic focusing. Where $y = y_{ex}(x)$ is the locus for varying R at which a straight line through the fixed point (e, d) touches the circle of radius R which is tangent to the y-axis at the origin.

$$y_{ex} = [xd \pm x(d^2+e^2-x^2)^{1/2}]/(e+x). \quad (3)$$

A brief discussion of this curve is given in the appendix. Since all particles leaving the source in the negative y-direction up to a maximum momentum – this restriction only for $e > 0$ – hit the detector at the same point, these magnets can really be

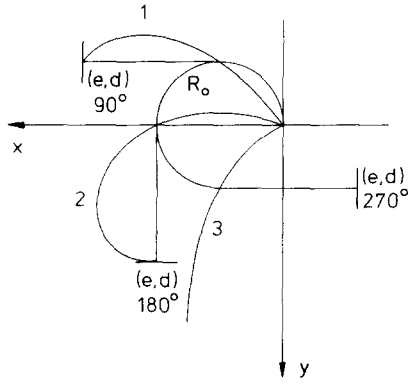

Fig. 1. The curves $y - y_{ex}$ for $\varphi_0 = 90°$ (1), 180° (2), 270° (3), and the corresponding central rays ($R_0 = 30$ mm, $B = 65$ mm). For $e > 0$, y_{ex} is plotted only to the position (e, d) of the detector.

* V. P. Belov et al.[4]) use $n < 0$ for achromatic bending of parallel beams, but strong vertical defocusing for divergent beams.

called non-dispersive. As an example, the curves y_{ex} for three arbitrarily chosen positions (e, d) of the detector (origin of the image coordinate system) are shown in fig. 1.

2.3. Spatial focusing

After the energetic focusing problem has been solved analytically, the next step is the connection of the linear theory to eq. (3). Since the linear theory is valid only for a straight pole boundary, its application requires the local substitution of y_{ex} by its tangent. If this is done for each trajectory with radius R (each point of y_{ex}), h_{12} and v_{12} are given by inserting:

$$\varphi = \arccos\{[(R^2-eR-d\,(e^2-2eR+d^2)^{1/2}]/ /[(e-R)^2+d^2]\}$$

$$\beta = \varphi-\pi-\arctan\{ed/(e+x)^2 \pm \pm(ed^2+e^3-2ex^2-x^3)/ /[(e+x)^2\,(d^2+e^2-x^2)^{1/2}]\} \quad (4)$$

$$b = [(x-e)^2+(y-d)^2]^{1/2}/R$$

(x, y) point of the curve $y = y_{ex}(x)$.

Since $h_{13} \equiv 0$ by eq. (3), the notation "central ray" loses its meaning, at least regarding the momentum deviation. In spite of the arbitrariness of the definition of R_0 and the corresponding values of φ and β, the usual notation of the linear theory has been retained for sake of the visualization. But it should be kept in mind that now the image point (e, d) and A and α are the only quantities which characterize the magnet. Fig. 2 illustrates the focusing properties of the corresponding magnets, calculated with eqs. (1), (3) and (4). The origin of the right-handed object coordinate system (in) lies at (O, A) in the x–y system of fig. 1; z_{in} is in the negative y-direction. The image coordinate system (out) is obtained by translating z_{in} along the curve of the central ray to the position (e, d).

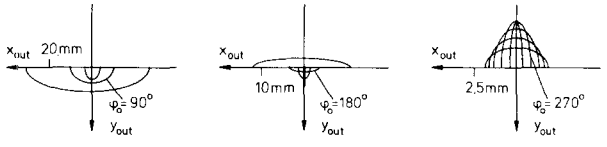

Fig. 2. Image coordinates of particles, which start with 1° ($y'_{in} \geq 0$) divergence and 1 mm distance from the origin of the object coordinate system. That is, the contour is obtained by varying the azimuth about the z_{in}-axis from 0 to π. $A = 120$ mm, $\alpha = 20°$ ($\varphi_0 = 90°, 180°$) and 35° ($\varphi_0 = 270°$); $\delta = -50\%$, 0%, 50%, 100%, 150%. With increasing δ, x_{out} decreases for $\varphi_0 = 90°$, 180° and increases for $\varphi_0 = 270°$. According to the geometry (see fig. 1) some of the higher momenta are missed for $\varphi_0 = 90°$, 180° (note the different scales!).

2.4. Optimization procedure

To search for the best triple focusing magnet (minimum size of the focus and maximum momentum band) by means of eqs. (1), (3) and (4) would exceed the limits of the linear theory. In addition, it would be of little practical interest, if for example the positions of the source and the detector are determinated by the experiment. Against that, the following procedure allows the design of a magnet, which matches the experimental conditions. At the same time the dependence of the focus upon the different parameters is indicated, so that better results can be obtained eventually by changing some of the free parameters.

If one divides the momentum band $R_{max} \ldots R_{min}$ into m steps and chooses for the gauge the "averaged diagonal"

$$F_m = \frac{1}{m}\sum_{i=1}^{m}\{[h_{12}^2(R_i)+v_{12}^2(R_i)]^{1/2}\,R_i\}, \quad (5)$$

one has to find:

$$F_m\,(R_0, \varphi_0, A, B_0, \alpha) = \min \quad (6)$$

(Index 0 means $\delta = 0$, $R_i = R_0 + \delta_i R_0$).

Various calculations showed that the gauge, eq. (5), is better suited for predicting the quality of the magnet than for instance the standard deviation or the maximum of the matrix elements h_{12} and v_{12}. The values for m and δ_i can be chosen individually. In the present case the standard was: $m = 3$, $\delta_i = -30\%$, 0%, 150%.

In contrast to the above mentioned solutions of system (2), now only β_0 is fixed by the curve y_{ex}, eq. (3). But this curve in turn yields a non-dispersive magnet in the SCOFF-approximation, and four (instead of two) free parameters can be used to optimize the spatial focusing. To do that, the positions of the source and the detector are varied within the areas given by the experimental arrangement. Then for each position the best magnet design is calculated according to eq. (6). In our special case first calculations on a PDP 11-45 showed that for $R_{max}/R_{min} = 3{,}6$ the size of F_m only for $\varphi_0 > 220°$ becomes sufficiently small. For the completion of the results that were gained from separate points (R_0, φ_0, A, B_0, α), the function $F_m(R_0, \varphi_0)$ was computed with the remaining quantities as parameters. From the figs. 3 and 4 it

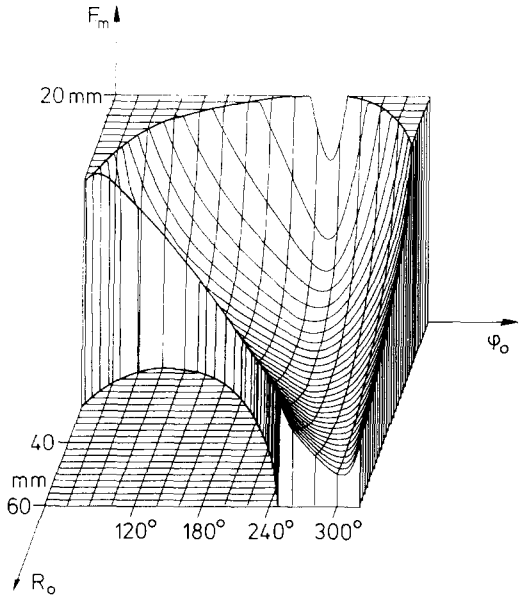

Fig. 3. The function $F_m(R_0, \varphi_0)$. A = 130 mm, α = 20°, B = 65 mm, δ = −30%, 0%, 150%. For complex values of F_m (cf. eqs. (3), (4) and figs. 1 and 2) F_m is set to zero.

can be seen that only one minimum of $F_m(R_0, \varphi_0)$ exists. This minimum travels diagonally towards greater values of φ_0 and R_0, if α and B_0 are increased. Simultaneously the "valley" becomes narrower and deeper. However, the main purpose of these calculations was to make sure that no considerably better values of F_m result if the parameters are slightly changed, i.e. that no sharp minima exist. The result of the linear optimization is given in table 1(a).

3. Optimization to higher order

Concerning the momentum deviation, the limitation of the linear theory has been bypassed with the eqs. (3) and (4). But there rests an uncertainty when greater divergences are desired. Moreover, as a consequence of larger solid angles larger gaps are needed, so that the SCOFF-approximation

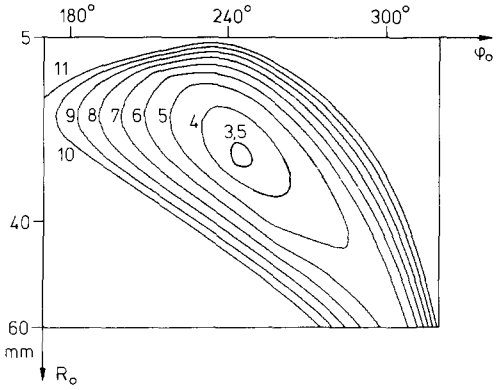

Fig. 4. Diameter (in mm) of the focus for ± 1° divergence at the input (corresponds to $2F_m$). The iso-lines were plotted by means of the program AEQUI, provided from the Lehrstuhl für Theoretische Elektronenphysik der Universität Tübingen.

may break down. Therefore, the second step of the optimization was the numerical integration. The "ray-tracing program"[9]), which was generously released to us by MIT and somewhat altered due to the large values of φ and δ and to make it compatible with the CDC 3300, was used for computing and plotting the electron trajectories.

The extended fringing field (EFF) is described by:

$$B = B_0/[1 + \exp(S)],$$
$$S = C0 + C1 \cdot s + \ldots + C5 \cdot s^5, \qquad (7)$$
$$s = z/D \ (D = \text{gap width}),$$

where the coeffcients were evaluated by fitting the field of a test magnet with straight boundary, but otherwise identical with the designed magnet. With

$$C0, \ldots, C5: 6.190 \times 10^{-1},\ 2.181,\ -5.088 \times 10^{-1},$$
$$6.639 \times 10^{-1},\ -3.875 \times 10^{-1},$$
$$7.139 \times 10^{-2},$$

the deviation from the measured field is less than one percent.

The curve $y = y_{ex}(x)$ can be approximated in the

TABLE 1

Steps of optimization. Lengths in mm, angles in degree. Unchanged data: gap width: D = 1.5 cm, width of pole pieces: 2 cm, coil cross section: $2 \times 2\ \text{cm}^2$, thickness of yoke: 1 cm.

	R_0	φ_0	α	A	B_0	β_0	curvature
a)	25	264	35	130	80	30.5	entrance: straight exit: y_{ex}
b)	20	264	33	120	64	30.5	entrance: $S2, \ldots, S8$
$S2, \ldots, S8$:	-3.573×10^{-2}	4.948×10^{-4}	-3.524×10^{-3}	1.212×10^{-4}	1.644×10^{-4}	-2.567×10^{-5}	1.175×10^{-6} exit: R_c = 95 mm
c)	20	266	34	120	65	34	entrance and exit:
d)	20	269	36	120	65	36	R_c = 95 mm

ray-tracing program by a polynomial

$$z = S2 \cdot x^2 + S3 \cdot x^3 + \ldots + S8 \cdot x^8 \qquad (8)$$

in the coordinate systems B and C (see fig. 5 or 6a) or by circles.

The possibility to produce the desired field by straight pole boundaries and correction provisions such as external coils or field clamps has not been used. Rather, coils are wound that follow the surface of the pole pieces even for concave curvature (see fig. 5). This frees one from lengthly field measurements and calculations, and yields a compact device structure.

In the second step the magnet data were changed as can be seen from table 1(b). In comparing calculations I demonstrated that for large deflecting angles the different curves corresponding to entrance and exit boundaries may be replaced by a single circle (see fig. 1) without substantial loss in focusing. Because this facilitates the manufacturing of the pole pieces, a possible enlargement of the focus (about 2 mm) was allowed. The resulting magnet is represented in fig. 5 and its data in table 1(c). As a further emphasis, it may be pointed out that a *circular* pole shape always implies $\alpha = \beta$, but it is not a sufficient condition for triple focusing. The differences from the symmetrical magnet with *straight* boundaries are shown in the discussion.

4. Experimental testing

The calculations necessarily contain errors (from the field measurements up to the applied numerical methods) and it would be a cumbersome task to eliminate these inaccuracies by constructing a series of magnets. But a part of that series can be simulated if the position of the magnet is varied. Therefore, a testing chamber was constructed in which the source, the magnet, and the detector could be rotated within wide ranges and shifted from outside the chamber. A divergent beam was produced by 100 keV electrons scattered from an Au-target. Representative rays were selected, and photographically observed and compared with the computed trajectories. Agreement was found within the accuracy of the measurement of the particle coordinates (about ± 0.5 mm), except for the highest momenta. (They had to be simulated by such low currents that the remanent field of the ordinary steel employed could no longer be neglected, and better (!) horizontal focusing results). A part of the selected rays is shown in fig. 5 and 6. Be-

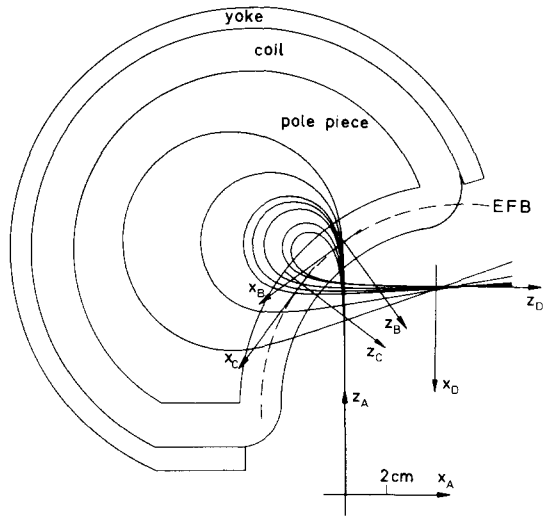

Fig. 5. Designed magnet [table 2(d)] and particle trajectories with $\delta = 160\%$, 65%, 12%, 0%, -15%, -41%, -56%. (EFB = effective field boundary.)

sides that control, a last improvement became possible by a small displacement of the magnet in the x_A-direction [corresponding data see table 1(d)]. Fig. 7 serves as a visual completion to fig. 5 and

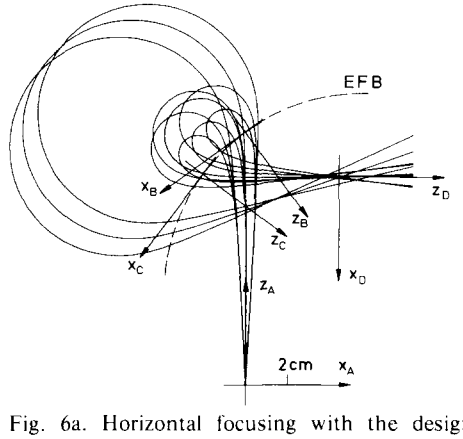

Fig. 6a. Horizontal focusing with the designed magnet for $\delta = 160\%, -15\%, -56\%$, with $0°$, $\pm 3°$, respectively (the central ray is added); for the rest see table 2(d).

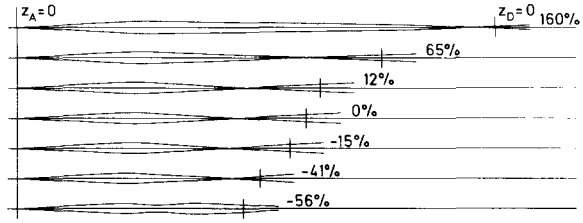

Fig. 6b. Vertical focusing with the designed magnet, $\pm 3°$, δ as noted. The dashes at $z_D = 0$ correspond to 2 cm, same scale for y- and z-direction.

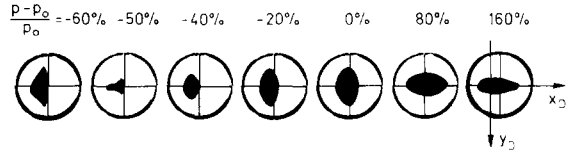

Fig. 7. Images of a 1 mm diameter spot, observed under 7.6 msr (annular diaphragm). A circle of 1 cm ∅ has been cut out of the fluorescent screen and was illuminated from the rear during exposure. If the center of the circle (detector) lies at $x_D = 1.5$ mm, all images are well inside the circle.

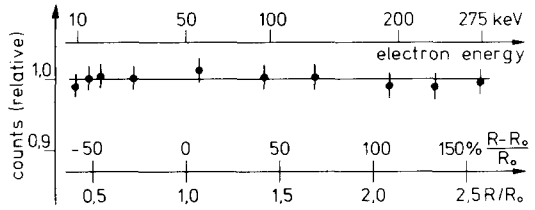

Fig. 8. Counting rate vs. electron energy. Obtained with a 10 mm ∅ SB-detector when electrons which have undergone elastic scattering (Mott-scattering) are observed with a solid angle of 7.6 msr. Electron energy 300 keV, scattering angle 57°. Different energies are simulated by varying the field strength. Only the statistical errors are shown.

6. The behaviour of the entire apparatus, i.e. the combination of the magnet with a SB-detector, was tested under the final experimental conditions. The correct simulation of the electron energy was checked once more by recording the Ba 133 conversion electron spectrum (45–380 KeV). In the meantime ELSA is in action in a two parameter measurement of the elementary process of e–e bremsstrahlung within the energy range indicated in fig. 8.

5. Discussion

A magnet was designed which focuses electrons within a momentum band of $p_{max}/p_{min} = 5.9$ and a solid angle of 7.6 msr onto a detector with a maximum diameter of 10 mm. To obtain these demanding values, the requirement for zero-dispersion was connected to the linear theory in such a way that most of the variables characterizing the magnet remained free for the optimization. The steps of the development were: a) linear optimization, b) regard of the extended fringing field, c) construction with simplified (circular) curvature, d) correction by experimental testing (see table 1). Fig. 9 impressively confirms the limitations of the results obtained by means of the *solution* of system (2). It also shows that a symmetrical magnet [$\alpha = \beta$, $a = b$, as designed by H. Ejiri et al.[5])] is not a sufficient condition for optimum triple focusing. However, the result of the procedure LOAD may be justly called "non-dispersive". Looking at the spatial focusing properities of ELSA and noting that they are improved too, it is clear that optimizing was worthwhile. Or in other words: $\varphi = 270°$ is not only a practical deflection angle, but also makes good triple focusing possible, if the pole pieces have the appropriate curvature. Finally, it may be worth mentioning that $|h_{11}|$ and $|v_{11}|$ are still near unity.

Undesired momenta can be cut off sufficiently sharp (the counting rate falls to 50%, if the momentum is changed by 5% in average) at the intermediate horizontal focus (see fig. 6a) at least down to $\delta = -15\%$. Therefore, intermediate *double* focusing seems to be unnecessary. Moreover, if the momenta of the perturbing particles lie not too close to $\delta = 160\%$ or $\delta = -60\%$, ELSA may act

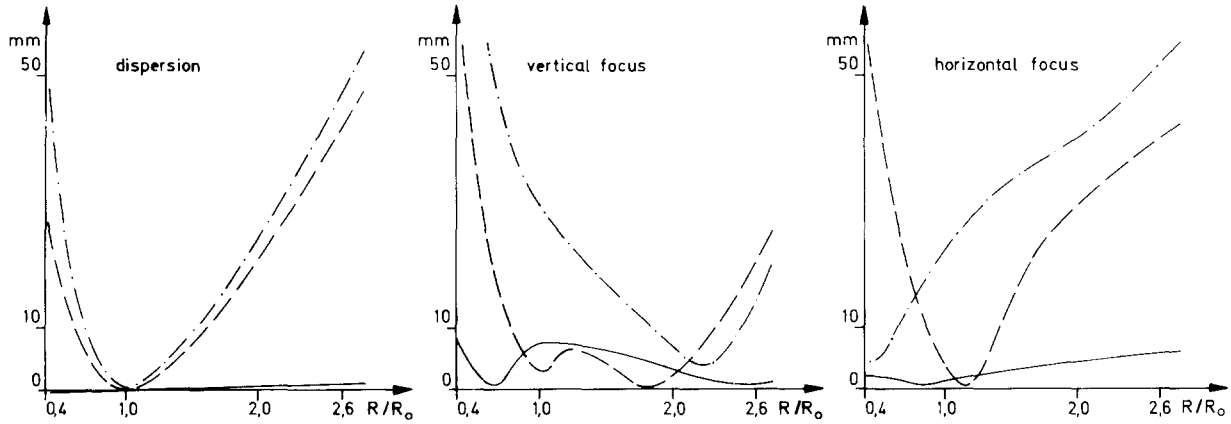

Fig. 9. Focusing properties. The image coordinates were calculated with the ray-tracing program[9]). Dispersion: Deviation of the central ray from $x_D = 0$, vertical and horizontal focus: distance between ± 3° rays at $z_D = 0$. –·–: $\varphi = 270°$, H. A. Enge[7]), – –: TESS, H. Ejiri et al.[5]), ——: ELSA.

without any additional precautions. This is possible because vertical defocusing increases rapidly at the low momentum end (see fig. 9), whereas at the other end the particles approach the field boundary inside the magnet (see fig. 5), which causes sudden dispersion. In this way energy ranges like 10–275 keV, 40–700 keV, or with cooled coils 125–1800 keV may be observed simultaneously and under a reasonable solid angle. Using a premium SB-detector, which was cooled by a Peltier-element to about 0 °C, we get 5 keV and 8 ns [SB vs Ge(HP)] for typical resolutions.

If smaller ranges, for instance $p_{max}/p_{min} = 1.5$ are adequate, but the positions of the source and the detector demand smaller deflection angles, a satisfactory result may be obtained any way with LOAD (see figs. 3 and 4). A new magnet of this type is in development for the observation of the second electron produced in e–e bremsstrahlung in a threefold coincidence experiment.

I am indebted to Dr. W. Nakel who initiated this work and gave much helpful advice. I wish to thank Prof. Dr. E. Kasper for helpful discussions on electron optics and Dr. S. B. Kowalski of MIT for providing the "ray-tracing program". This work was supported by the Deutsche Forschungsgemeinschaft.

Appendix

Especially when programming eq. (3), there are several points which must be treated carefully:

1) For $x^2 > e^2 + d^2$ the value of y_{ex} becomes complex. If $e > 0$ and $x > 0$ this means that the detector lies within the circle.
2) The sign ambiguity in eq. (3) is best resolved for each point (e, d) individually. (It is due to the fact that there exist two tangents from a point onto a circle.) Note that one curve which describes the curvature of the exit boundary can consist of more than one part.
3) For $x = -e$, y_{ex} has a pole with a sign change as well as the finite value e^2/d. This is of special interest if the trajectory crosses the incomming ray. In this case it may be necessary to construct the curve from three parts, each of them with the proper sign.

For the convenience of the reader the following programs are available from the author:

CUR0 2: Computation and plot of the curve $y = y_{ex}(x)$ (fig. 1) as well as a polynomial fit for the determination of the coefficients $S1, \ldots, S8$, which are needed in the ray-tracing program.

KOMPLOT: Computation and plot of the focusing contours (fig. 2).

LOAD: Computation and plot of the function F_m (fig. 3).

FOCUS: Iso-lines of the function F_m (fig. 4).

EXPO: Fit and plot of a measured fringing field, coefficients $C0, \ldots, C5$ for the ray-tracing program.

References

[1] R. C. Catura, Nucl. Instr. and Meth. **32** (1965) 152; J. Kantele, M. Luontama, A. Passoja and R. Julin, Nucl. Instr. and Meth. **130** (1975) 467.
[2] W. Nakel and E. Pankau, Z. Phys. **264** (1973) 139; Z. Phys. **274A** (1975) 319; Phys. Lett. **44A** (1973) 65.
[3] A. P. Banford, *The transport of charged particle beams* (E. & F. N. Spon Ltd., London, 1966).
[4] V. P. Belov and A. M. Kokorin, Soviet Phys.-Techn. Phys. **14** (1970) 1520.
[5] H. Ejiri, T. Shibata, Y. Nagai and S. Nakayama, Nucl. Instr. and Meth. **134** (1976) 107.
[6] R. A. Alvarez, K. L. Brown, W. K. H. Panofsky and C. T. Rockhold, Rev. Sci. Instr. **31** (1960) 556.
[7] H. A. Enge, *Focusing of charged particles* (ed. A. Septier; Academic Press, New York, 1967) vol. 2, ch. 4.2.
[8] P. Ciuti and F. de Guarrini, Nucl. Instr. and Meth. **98** (1972) 361.
[9] H. A. Enge and S. B. Kowalski, *Recent Spectrograph Design Work Utilizing a Fourth-order Ray-tracing Program*, Proc. 3rd Int. Conf. on *Magnet Technology*, 19/20.05.69, Hamburg (1970).